Time-Reversal Massive Multipath Effect: A Single-Antenna "Massive MIMO" Solution

Yi Han, *Student Member, IEEE*, Yan Chen, *Senior Member, IEEE*, Beibei Wang, *Senior Member, IEEE*, and K. J. Ray Liu, *Fellow, IEEE*

***Abstract*— The explosion of mobile data traffic calls for new efficient 5G technologies. Massive multiple-input multiple-output (MIMO), which has shown the great potential in improving the achievable rate with a very large number of antennas, has become a popular candidate. However, the requirement of deploying a large number of antennas at the base station may not be feasible in indoor scenarios due to the high implementation complexity. Does there exist a good alternative that can achieve similar system performance to massive MIMO for indoor environment? In this paper, we show that by using time-reversal (TR) signal processing, with a sufficiently large bandwidth, one can harvest the massive multipaths naturally existing in a rich-scattering environment to form a large number of virtual antennas and achieve the desired massive multipath effect with a single antenna. We answer the above question by analyzing the TR massive multipath effect and the achievable rate with some waveforms. We also derive the corresponding asymptotic achievable rate under a massive multipath setting. Experiment results based on real indoor channel measurements show that the massive multipaths can be revealed with a sufficiently large bandwidth in a practical indoor environment. Moreover, based on our experiments with real indoor measurements, the achievable rate of the TR wideband system is evaluated.**

***Index Terms*— Time-reversal (TR), time-reversal division multiple access (TRDMA), time-reversal massive multipath effect (TRMME), massive MIMO.**

I. Introduction

WHILE the past few decades has witnessed the monumental success of mobile and wireless access to the Internet, the proliferation of new mobile communication devices, such as smartphones and tablets, has in turn led to an exponential growth in network traffic. According to the most recent Cisco Visual Networking Index (VNI) annual report [1], the global mobile data traffic grew 74% and the number of mobile devices increased more than half a billion (563 million) in 2015. The demand for supporting the fast-growing consumer data rates urges the wireless service providers and researchers to seek a new efficient radio access technology, which is the so-called 5G technology, beyond what current 4G LTE can provide. Besides ultra-densification and mmWave, massive multiple-input multiple-output (MIMO) is one of "big three" 5G technology [2], which can offer multi-fold benefits such as enormous enhancement in spectral efficiency and power efficiency [3] and simple transmit/receiver structures due to the quasi-orthogonal nature [4]. These benefits make massive MIMO one of the five disruptive technology directions for 5G communication [5].

Even though the benefits of massive MIMO seem very promising, several critical challenges must first be addressed before it can be implemented in practice. First of all, a challenging task is the analog front-end design [6], for example, each tiny antenna needs its own power amplifier and analog-to-digital convertor (ADC). Moreover, the antenna correlation and mutual coupling due to the increasing number of antennas have to be carefully addressed as well [7], [8]. The researchers in Lund University built a 100-antenna MIMO testbed, and the size is $0.8 \times 1.2 \times 1$ m with 300kg weight and 2.5kW average power consumption [9]. Considering the requirement of deploying a large amount of antennas, massive MIMO system has a high implementation cost in indoor scenarios. It is expected that 95% of data traffic will come from indoor in a few years [10], therefore a natural question to ask is: does there exist a good alternative that can achieve similar system performance to massive MIMO for indoor environments? The answer is yes and the time-reversal (TR) technology is potentially a counterpart of massive MIMO in indoor scenarios.

It is well known that radio signals will experience many multipaths due to the reflection from various scatters, especially in indoor environments. TR's focusing effect is in essence a spatial-temporal resonance effect that brings all the multipaths to arrive at a particular location at a specific moment. Such a phenomenon will allow us to utilize the naturally existing multipaths as virtual antennas to realize the massive multipath effect, which is a counterpart of massive MIMO effect, even with a single antenna. As shown in Fig. 1, TR inherently treats the multipaths in the environment as virtual antennas, similar to MIMO that uses multiple antennas for better spatial multiplexing. In essence, if cooperation of users, e.g. cooperative communications, is a distributed way of achieving MIMO effect of high diversity, then TR is similarly a distributed way to achieve the massive MIMO effect through utilizing the multipaths as virtual antennas. The TR waveform is nothing but to control each multipath (virtual antenna).

In order to harvest the multipaths, the transmit power and bandwidth can be utilized. More specifically, the maximum

Manuscript received December 12, 2015; revised April 9, 2016 and June 8, 2016; accepted June 16, 2016. Date of publication June 22, 2016; date of current version August 12, 2016. The associate editor coordinating the review of this paper and approving it for publication was Y. J. Zhang.

Y. Han, B. Wang, and K. J. R. Liu are with the University of Maryland, College Park, MD 20742 USA, and also with Origin Wireless Inc., Greenbelt, MD 20770 USA (e-mail: yhan1990@umd.edu; bebewang@umd.edu; kjrliu@umd.edu).

Y. Chen is with the University of Electronic Science and Technology of China, Chengdu 610051, China, and also with Origin Wireless Inc., Greenbelt, MD 20770 USA (e-mail: eecyan@uestc.edu.cn).

Color versions of one or more of the figures in this paper are available online at http://ieeexplore.ieee.org.

Digital Object Identifier 10.1109/TCOMM.2016.2584051

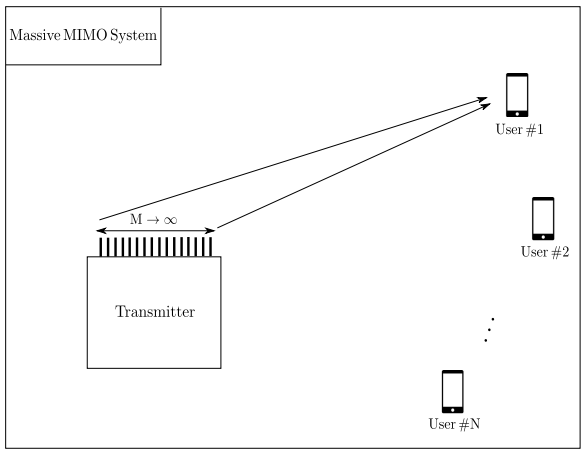

(a)

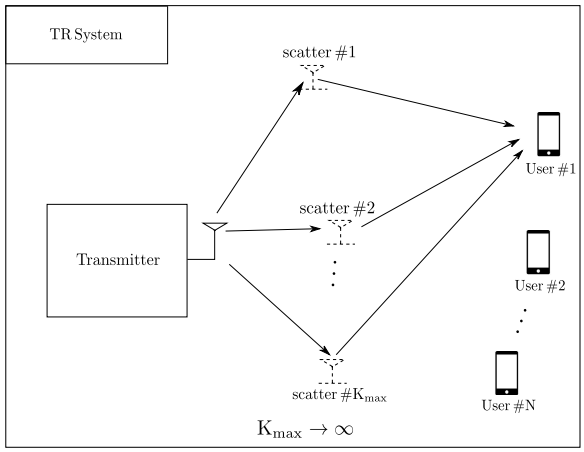

(b)

Fig. 1. Comparison between massive MIMO and TR system. (a) Massive MIMO system. (b) TR system.

number of observable multipaths given by an environment increases with the transmit power. Once the power is fixed, the maximum number of observable multipaths is also fixed. In addition, more multipaths can be resolved with the increase of bandwidth because of the better time resolution. Based on the real indoor ultra-wide-band (UWB) channel measurement (both LOS and NLOS) in [11] and [12], around 60-80 independent multipaths can be revealed with a sufficiently large bandwidth. Later in Section VI, we will discuss about how to realize the massive multipath in a practical indoor environment.

TR technology is a promising candidate for indoor communication, but it requires large bandwidth to achieve good time resolution. The wideband signal naturally requires the high sampling rate based on the Nyquist samping theorem, which leads to heavy computation burden in terms of processing. Fortunately, as indicated by Moore's Law, the more powerful ADC and digital signal processor (DSP) reduce the wideband signal processing cost dramatically [13]. Moreover, researchers and engineers are currently searching for new available wide band and re-allocating bandwidth for 5G technology [2]. For TR technology, it may use the spectrum of ultra-wide-band (UWB) or mmWave band. Based on the existing study at high frequencies, there still exists a large amount of multipaths, which is essential for TR communication. For example, based on the building penetration and reflection measurements on 28GHZ in NYC [14], the RF energy is mostly retained within buildings due to low attenuation and high reflection through indoor materials. Moreover, the delay spread for indoor 60GHz channels ranges between 30ns and 70ns [15], which indicates a multipath-rich environment. Even though the spectral efficiency of TR technique is not that high, it becomes more and more important to reduce complexity, operation energy consumption and offer other benefits given the potential wide bandwidth, especially in indoor scenarios.

By exploiting the massive number of virtual antennas, TR system can achieve superior focusing effect in spatial-temporal domain, resulting in the promising performance as an indoor communication candidate for 5G. Moreover, the implementation complexity of TR system is much lower since it utilizes the environment as the virtual antenna array and computing resource. Specifically, in this paper, we consider a Time-Reversal Division Multiple Access (TRDMA) downlink communication system [16] to demonstrate the TR massive multipath effect (TRMME). We further derive the asymptotic achievable rate performance under typical waveforms, i.e., the basic TR, zero-forcing (ZF) and minimum mean square error (MMSE) waveforms as the number of observable multipaths becomes sufficiently large. Later, we discuss the approach to realize massive multipaths based on real-world indoor channel measurements. Through the experiments with real indoor measurements, the achievable rate of a TR wideband system with a single antenna is evaluated.

The rest of this paper is organized as follows. We first discuss the existing related work in Section II. The system model is discussed in Section III. In Section IV, the notion of TRMME is introduced assuming that the TR system has the ability to reveal massive multipaths in a rich-scattering environment. In Section V, the expected achievable rate of the TR system with typical waveforms are investigated. Moreover, the asymptotic achievable rates with these waveforms is derived in a massive multipath setting. The approach to realize massive multipaths in a practical indoor environment is discussed based on the real-world channel measurements in Section VI. Finally, Section VII concludes the paper.

Notations: $|\cdot|$, $(\cdot)^T$ and $(\cdot)^\dagger$ stand for absolute value, transpose and conjugate transpose, respectively. The boldface lowercase letter $\mathbf{a}$ and the boldface uppercase letter $\mathbf{A}$ represent vector in column form and matrix, respectively. $\|\mathbf{a}\|$ denotes the Euclidean norm of a vector. $\mathbf{a}^{[D]}$ denotes the up-sampled vector by inserting $D-1$ zeros between two adjacent elements in the vector $\mathbf{a}$. We denote $(\mathbf{a} * \mathbf{b})$ as the linear convolution between two vectors $\mathbf{a}$ and $\mathbf{b}$. $[\mathbf{A}]_{m,n}$ stands for the element in the m^{th} row and the n^{th} column of the matrix $\mathbf{A}$. Finally, we denote $\xrightarrow{d}$ as the convergence in distribution.

II. Related Work

The TR technology was first introduced to compensate the delay distortion on wired transmission lines by Bogert from Bell Labs in the fifties [17]. More recently, TR has drawn more and more attention from researchers in the wireless

communications field [18]–[20]. Under a rich-scattering environment, a TR communication system is shown to have the spatial-temporal focusing effect and thus work as an ideal platform for green wireless communications [21], [22] in terms of lower power consumption and less radio pollution. A TRDMA scheme is proposed in [16] which utilizes the location-specific waveform to separate different users' signal. It is shown in [16] and [23] that the TR communication system can be extended to multiple-antenna scenarios easily, and more advanced waveform design can be implemented to further suppress the inter-symbol-interference (ISI) and inter-user-interference (IUI) to achieve higher data rate [24], [25]. The potential application of TR technology in the Internet of Things is discussed in [26].

Time-Reversal is neither a new terminology in MIMO technology as well. First of all, time-reversal beamforming is well known as conjugate beamforming in MIMO systems when the system bandwidth is small [27]. Then, for wide-band, frequency-selective channel, OFDM can rigorously decompose the channel into parallel independent narrow-bandwidth sub-carriers, where TR precoding can be applied [28], [29]. TR can be also employed as the precoding scheme directly for a single carrier wideband system [30], [31].

The focus of this paper is not on the combination of massive MIMO and TR technologies. Instead, we show that TR technology itself is a promising approach to realize the massive multipath effect, which is similar to massive MIMO effect, for indoor communications. Together with the theoretic analysis of the TRMME, the idea of realizing massive virtual antennas with a single physical one and the approach to resolve the multipaths with the increase of bandwidth in an indoor environment constitute the novelty of our paper.

III. System Model

In this paper, we consider a time-reversal downlink system where one transmitter simultaneously communicates with N distinct receivers through the TRDMA technique [16]. We assume that both the transmitter and receivers are equipped with one single antenna. However, the results can be easily extended to the multiple-antenna scenario.

A. Channel Model

Suppose there are totally K_{max} independent multipaths from the transmitter to the j^{th} receiver, then the channel $h_j(t)$ can be written as

$$h_j(t) = \sum_{k=1}^{K_{max}} \tilde{h}_{j,k}\delta(t-\tau_k), \tag{1}$$

where $\tilde{h}_{j,k}$ and τ_k are the complex channel gain and path delay of the k^{th} path, respectively. Note that the delay spread of the channel is given by $\tau_C = \tau_{K_{max}}$.

Let W be the bandwidth of the TR system. Through Nyquist sampling, the discrete channel responses is

$$h_j[n] = \int_{n\tau_p-\tau_p}^{n\tau_p} p(n\tau_p-\tau)h_j(\tau)d\tau, \tag{2}$$

where $p(t)$ is the pulse with main lobe $\tau_p = 1/W$.

Through (2), a L-tap channel $\mathbf{h}_j = [h_j[1], h_j[2], ..., h_j[L]]^T$ with $L = round(\tau_C W)$ can be resolved for the link between the transmitter and the j^{th} receiver as follows

$$\mathbf{h}_j = \left[h_{j,1}, h_{j,2}, \cdots, h_{j,L}\right], \tag{3}$$

where $h_{j,i}$ is the complex channel gain of the i^{th} tap, and $h'_{j,i}s$ are independent for all $i \in [1, L]$ and $j \in [1, N]$.

Suppose that there are K non-zero elements in the L-tap channel $\mathbf{h}_j$. When the bandwidth W is small, all elements in $\mathbf{h}_j$ are generally non-zero, i.e., $K = L$. On the other hand, when W is sufficiently large, the side lobes of $p(t)$ becomes negligible and thus there are at most $K = K_{max} < L$ non-zero elements in $\mathbf{h}_j$. Let $\phi_{K_{max}}$ be the non-zero multipath set, which reflects the physical patterns of scatter distribution in the environment. Then, $h_j[k] = 0$ for $k \notin \phi_{K_{max}}$, and for $k \in \phi_{K_{max}}$, $h_j[k]$ is a complex random variable with zero mean and variance σ_k^2.

Prior to the TR-transmission, a pseudo random sequence is sent to the transmitter from the receiver, based on which the channel state information (CSI) $\mathbf{h}_j$ is estimated. By cross-correlating the received signal with the known pseudo random sequence, the power of CSI is boosted thus maintaining the good CSI quality. Due to the more powerful DSP and the efficient Golay correlator [32], the CSI estimation is obtained quickly in terms of time consumption by converting the multiplication operation into addition/substruction. In addition, based on the real measurement in [33], the CSI is quite stationary given only slightly changing of the environment, which indicates the channel need not to be re-probed very frequently and the overhead price of channel probing is very small.

Note that pilot contamination, when a lot of users simultaneously channel probe to the base station, will cause the performance degradation in the TR system due to the non-ideal CSI. In the following, we assume the estimated CSI is perfect.

B. TRDMA Downlink Communication

In the TR system, the transmitter simultaneously communicates with multiple receivers. Specifically, as shown in Fig. 2, the information to be transmitted to the j^{th} receiver, denoted as X_j, is first up-sampled by a backoff factor D to alleviate the interference, and then precoded by a waveform $\mathbf{g}_j$. Actually, the symbol rate is lower down by D to suppress the ISI caused by the multipath channel. Note that multiple designs of the waveform such as basic TR waveform [21], zero-forcing (ZF) waveform [34] and minimal mean square error (MMSE) waveform [24] can be utilized, and the details will be discussed in the next section. After that, all signals to different receivers are mixed together as follows

$$S[k] = \sum_{i=1}^{N} \left(X_i^{[D]} * \mathbf{g}_i\right)[k], \tag{4}$$

where

$$X_i^{[D]}[k] = \begin{cases} X_i[k/D], & \text{if } mod(k, D) = 0, \\ 0, & \text{otherwise.} \end{cases} \tag{5}$$

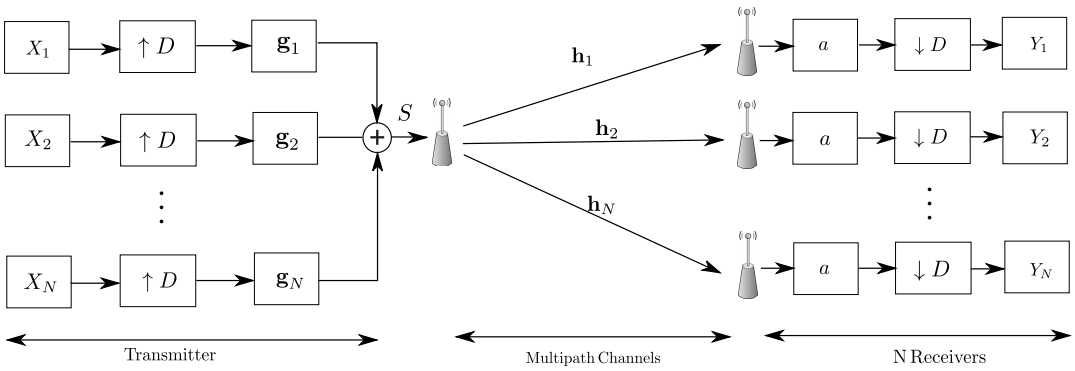

Fig. 2. A TRDMA System.

The mixed signal is broadcast to all receivers through the rich-scatter environment. At the receiver side, the j^{th} receiver simply scales the received signal and down-samples it to obtain the estimated signal Y_j as follows

$$Y_j[k] = (\mathbf{h}_j * \mathbf{g}_j)[L]X_j[k - \frac{L}{D}] + \sum_{l=1, l\neq L/D}^{\frac{2L-1}{D}} (\mathbf{h}_j * \mathbf{g}_j)[Dl]X_j[k-l] + \sum_{i=1, i\neq j}^{N} \sum_{l=1}^{\frac{2L-1}{D}} (\mathbf{h}_j * \mathbf{g}_i)[Dl]X_i[k-l] + n_j[k]. \quad (6)$$

Without loss of generality, we assume with the typical waveforms $(\mathbf{h}_j * \mathbf{g}_j)$ has the resonating effect at time index L. Then the first term in (6) is the desired signal, the second term is the ISI, the third term is the IUI, and the last term is the noise.

The (6) can be re-written by replacing the convolution as inner product as follows

$$Y_j[k] = \mathbf{H}_j^{(\frac{L}{D})}\mathbf{g}_j X_j[k - \frac{L}{D}] + \sum_{l=1, l\neq L/D}^{(2L-1)/D} \mathbf{H}_j^{(l)}\mathbf{g}_j X_j[k-l] + \sum_{l=1}^{(2L-1)/D} \mathbf{H}_j^{(l)} \left(\sum_{i=1, i\neq j}^{N} \mathbf{g}_i X_i[k-l] \right) + n_j[k], \quad (7)$$

where $\mathbf{H}_j^{(m)}$ is the m^{th} row of the $(2L-1)/D \times L$ matrix $\mathbf{H}_j$ decimated by rows of Toeplitz matrix, which can be written in (8), as shown at the bottom of this page. Therefore, $\mathbf{H}_j^{(\frac{L}{D})}$ is the time-reversal channel, i.e.,

$$\mathbf{H}_j^{(\frac{L}{D})} = \Big[h_j[L]\, h_j[L-1] \cdots h_j[1] \Big]. \quad (9)$$

C. Expected Achievable Rate for Individual User

Let P and P_n be the average transmitting power and noise power, respectively, and $(\cdot)^\dagger$ represent the conjugate transpose operator. According to (7) and the uplink-downlink duality [35]–[37], the achievable rate of the j^{th} receiver can be derived using its dual uplink format, where the uniform power allocation is assumed. Then we take an expectation of the downlink achievable rate as shown in (10), as shown at the bottom of this page. In the rest of the paper, we analyze the expected achievable rate of the TR system.

IV. Time-Reversal Massive Multipath Effect

In this section, we derive a TRMME for the TR technique in a rich-scattering environment. Similar to the massive MIMO effect in massive MIMO given an excessive amount of antennas [4], the multipath profile of different users in the TR system will also be orthogonalized given massive independent multipaths. Considering the channel delay spread in wideband

$$\mathbf{H}_j = \begin{pmatrix} h_j[D] & h_j[D-1] & \cdots & h_j[1] & 0 & \cdots & \cdots & 0 \\ h_j[2D] & h_j[2D-1] & \cdots & \cdots & h_j[1] & 0 & \cdots & 0 \\ \vdots & \vdots & \ddots & \ddots & \ddots & \ddots & \ddots & \vdots \\ h_j[L] & h_j[L-1] & \cdots & \cdots & \cdots & \cdots & \cdots & h_j[1] \\ \vdots & \vdots & \ddots & \ddots & \ddots & \ddots & \ddots & \vdots \\ 0 & \cdots & 0 & h_j[L] & \cdots & \cdots & h_j[L-D+1] & h_j[L-2D] \\ 0 & \cdots & \cdots & 0 & h_j[L] & \cdots & h_j[L-D+1] & h_j[L-D] \end{pmatrix} \quad (8)$$

$$R_j = \frac{W}{D}\mathbb{E}\left[\log_2 \left(1 + \frac{\frac{P}{N}\mathbf{g}_j^\dagger \mathbf{H}_j^{(\frac{L}{D})\dagger}\mathbf{H}_j^{(\frac{L}{D})}\mathbf{g}_j}{\frac{P}{N}\mathbf{g}_j^\dagger \left(\mathbf{H}_j^\dagger \mathbf{H}_j - \mathbf{H}_j^{(\frac{L}{D})\dagger}\mathbf{H}_j^{(\frac{L}{D})} \right)\mathbf{g}_j + \frac{P}{N}\sum_{i=1, i\neq j}^{N} \mathbf{g}_j^\dagger \mathbf{H}_i^\dagger \mathbf{H}_i \mathbf{g}_j + P_n} \right) \right] \quad (10)$$

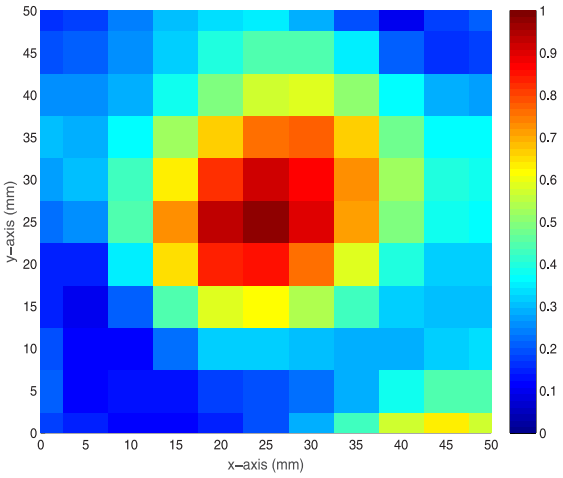

Fig. 3. The Spatial Focusing Ball with 125MHz Bandwidth.

system, the channel matrix considered in the following is the combination of decimated Toeplitz matrices in (8).

Theorem 1 (Time-Reversal Massive Multipath Effect): When K_{max} is sufficiently large, with the asymptotic setting that $W \to \infty$ to resolve all the multipaths, we have

$$\begin{cases} [\mathbf{Q}\mathbf{Q}^{\dagger}]_{m,n} & \xrightarrow{d} 0, \text{ if } m \neq n \\ \frac{[\mathbf{Q}\mathbf{Q}^{\dagger}]_{m,m}}{\lambda_m} & \xrightarrow{d} 1, \text{ otherwise,} \end{cases} \tag{11}$$

where $\mathbf{Q} = [\mathbf{H}_1^T, \mathbf{H}_2^T, \cdots, \mathbf{H}_N^T]^T$, $\xrightarrow{d}$ represents the convergence in distribution, and $\lambda_m = \|\mathbf{h}_j\|^2$ if $m = (j-1)(2L-1)/D + L/D$.

The proof for Theorem 1 is listed in the appendix. Since $\mathbf{Q}$ is the combination of CSIs from the transmitter to N receivers, the term $\mathbf{Q}\mathbf{Q}^{\dagger}$ represents the correlation matrix of these N CSIs. Therefore, the derived TRMME implies that the CSIs to N receivers become orthogonal to each other under the rich-multipath setting. Based on the indoor measurements with the TR prototype in [33], TR with 125MHz bandwidth is capable to formulate a spatial focusing ball as shown in Fig. 3. With the derived TRMME, the focusing ball of TR naturally shrinks to a pinpoint in a rich-scattering environment with a sufficiently large bandwidth, which is also predicted and observed in the massive MIMO system. Therefore, the derived TRMME is a counterpart of the massive MIMO effect in indoor scenarios.

In practice, we need that K_{max} is large enough to achieve the massive multipath effect. Based on the real indoor measurement in Sec. VI.B, we have demonstrated that the number of the resolved multipaths in a typical indoor environment is large enough given a sufficiently large bandwidth. Even though K_{max} is a fixed value given the power and environment, there still exist other methods to realize massive multipaths. Since the TR and MIMO technology are not mutually exclusive, the independent multipaths can be easily scaled up by adding a few antennas. How to realize massive multipaths is discussed with real indoor measurement later in Section VI. In the following, the asymptotic performance of TR technologies in a rich-scattering environment is derived based on the TRMME.

V. Expected Achievable Rate Under Different Waveforms

In this section, we analyze the asymptotic rates of TR technology. First, we derive the expected achievable rate under typical waveforms: basic TR waveform [21], ZF waveform [34] and MMSE waveform [24]. Then, the asymptotical achievable rate with the three waveforms is further derived based on the TRMME derived in Section IV.

A. Expected Achievable Rate

The three waveforms are shown in the following,

$$\mathbf{g}_j = \begin{cases} \mathbf{H}_j^{(L/D)\dagger} / \|\mathbf{H}_j^{(L/D)}\|, & \text{Basic TR} \\ c_{ZF}\mathbf{Q}^{\dagger}(\mathbf{Q}\mathbf{Q}^{\dagger})^{-1}\mathbf{e}_{l_j}, & \text{ZF} \\ c_{MMSE}(\mathbf{Q}^{\dagger}\mathbf{Q} + \frac{1}{p_u}\mathbf{I})^{-1}\mathbf{Q}^{\dagger}\mathbf{e}_{l_j}, & \text{MMSE} \end{cases} \tag{12}$$

where c_{ZF} and c_{MMSE} are normalization constants, $\mathbf{Q} = [\mathbf{H}_1^T, \mathbf{H}_2^T, \cdots, \mathbf{H}_N^T]^T$, $\mathbf{e}_{l_j}$ is an elementary vector with $l_j = (j-1)(2L-1)/D + L/D$, $\mathbf{I}$ is the identity matrix, and p_u is the transmitting signal-to-noise ratio (SNR) of each user defined as

$$p_u = \frac{P}{NP_n}. \tag{13}$$

With the definition of $\mathbf{Q}$ and $\mathbf{e}_{l_j}$ above, we have

$$\mathbf{Q}^{\dagger}\mathbf{e}_{l_j} = \mathbf{H}_j^{(L/D)\dagger}. \tag{14}$$

Note that under the multipath-rich scenario, ZF waveform can completely cancel out the interference given a large amount of independent multipaths. In addition, MMSE waveform has a simpler closed form solution with the fixed dual uplink power allocation [24].

Considering the more and more powerful DSP and the small time consumption of channel probing, the overhead of channel probing and waveform design is ignored in the following achievable rate analysis.

Theorem 2 (Expected Achievable Rate): The expected achievable rate of the TR system with basic TR waveform, ZF waveform, and MMSE waveform can be written as follows

$$\begin{aligned} R_j^{Basic} &= \frac{W}{D}\mathbb{E}\left[\log_2\left(1 + \frac{p_u\|\mathbf{h}_j\|^4}{p_u([\mathbf{Q}\mathbf{Q}^{\dagger}\mathbf{Q}\mathbf{Q}^{\dagger}]_{l_j,l_j} - \|\mathbf{h}_j\|^4) + \|\mathbf{h}_j\|^2}\right)\right], \\ R_j^{ZF} &= \frac{W}{D}\mathbb{E}\left[\log_2\left(1 + \frac{p_u}{[(\mathbf{Q}\mathbf{Q}^{\dagger})^{-1}]_{l_j,l_j}}\right)\right], \\ R_j^{MMSE} &= \frac{W}{D}\mathbb{E}\left[\log_2\left(\frac{1}{\left[\left(\mathbf{I} + p_u\mathbf{Q}\mathbf{Q}^{\dagger}\right)^{-1}\right]_{l_j,l_j}}\right)\right]. \end{aligned} \tag{15}$$

The proof for Theorem 2 is listed in the appendix. Note that the equations in Theorem 2 are not in closed-form due to the general channel model assumed in this paper. Theorem 2 serves as a starting point to derive the asymptotical expected achievable rate, which will be shown in later sections. Even though (15) seems similar to those for

MIMO MRC/ZF/MMSE receivers, the matrix $\mathbf{Q}$ is different from the channel profile matrix in MIMO system, which results in significantly different derivation of the asymptotical performance in the TR system. More specifically, due to the large channel delay spread in the TR system, there exists ISI. Therefore, backoff factor D is adopted in our paper and the channel profile $\mathbf{H}_i$ becomes the decimated Toeplitz matrix, which is much more complicated than that in MIMO system. Furthermore, it is the first work analyzing the asymptotical achievable rate for TR system with various waveform design methods with considering the ISI in practical system.

From Theorem 2, we can see that the expressions of expected achievable rate under different waveforms are closely related to $\mathbf{QQ}^\dagger$ and $\left[\mathbf{QQ}^\dagger\mathbf{QQ}^\dagger\right]_{l_j,l_j}$. Actually, the asymptotical property of $\mathbf{QQ}^\dagger$ has been studied previously as the TRMME. In the following section, we will further explore the property of $\left[\mathbf{QQ}^\dagger\mathbf{QQ}^\dagger\right]_{l_j,l_j}$ when K_{max} is sufficiently large, and study the corresponding asymptotic expected achievable rates with different waveforms.

B. Asymptotic Performance

We derive the asymptotic property of $\left[\mathbf{QQ}^\dagger\mathbf{QQ}^\dagger\right]_{l_j,l_j}$ in the following Lemma.

Lemma 1: When K_{max} is sufficiently large, under the asymptotic setting that $W \to \infty$ to reveal all the multipaths, we have

$$\lim_{W\to\infty} \sup \frac{\left[\mathbf{QQ}^\dagger\mathbf{QQ}^\dagger\right]_{l_j,l_j} - \|\mathbf{h}_j\|^4}{\sum_{k=1}^{K_{max}} \sigma_k^2} = \alpha, \tag{16}$$

where $\alpha = 2N/D$.

The proof for Lemma 1 is listed in the appendix. In a massive MIMO system, when the number of antennas grows large, the random channel vectors between the users and the base station become pairwisely orthogonal [38]. Similarly, in a TR system, when the number of multipaths grows, the random channel vectors between the receivers and the transmitter are also pairwise orthogonal, as shown in the TRMME. Different from the matched filter beamforming in massive MIMO system, basic TR waveform cannot completely remove the interference due to the channel delay spread in the wideband system. Therefore, the analysis of interference in Lemma 1 is needed for the derivation of the asymptotic expected achievable rate with basic TR waveform.

Based on the TRMME and Lemma 1, we can analyze the asymptotic expected achievable rate under different waveforms, and the results are summarized in the following Theorem.

Theorem 3: When K_{max} is sufficiently large, the asymptotic expected achievable rate under $W \to \infty$ with the ZF waveform and MMSE waveform satisfy that

$$\begin{aligned}\lim_{W\to\infty} \frac{R_j^{ZF}}{W/D} &= \lim_{W\to\infty} \frac{R_j^{MMSE}}{W/D} \\ &= \mathbb{E}\left[\log_2\left(1 + p_u\|\mathbf{h}_j\|^2\right)\right],\end{aligned} \tag{17}$$

while the asymptotic expected achievable rate with the basic TR waveform satisfies the following equation,

$$\lim_{W\to\infty} \inf \frac{R_j^{Basic}}{W/D} = \mathbb{E}\left[\log_2\left(1 + \frac{p_u\|\mathbf{h}_j\|^2}{\frac{p_u\alpha\left(\sum_{k=1}^{K_{max}}\sigma_k^2\right)^2}{\|\mathbf{h}_j\|^2} + 1}\right)\right]. \tag{18}$$

The proof for Theorem 3 is listed in the appendix. From Theorem 3, we can see that the ZF and MMSE waveforms generally outperform the basic TR waveform in terms of expected achievable rate. However, when D is sufficiently large so that $\frac{\alpha\left(\sum_{k=1}^{K_{max}}\sigma_k^2\right)^2}{\|\mathbf{h}_j\|^2}$ goes to zero, this is the case when the ISI and IUI are eliminated, then the basic TR waveform can achieve the same asymptotic expected achievable rate with ZF and MMSE waveforms.

VI. Simulations and Experiments

In this section, we conduct simulations and experiments to evaluate the expected asymptotical performance of a TR system under various settings. We assume that the N receivers are uniformly, randomly distributed and share the same channel model, which is discussed in Section III. Since more received power will be captured within the multipath-rich environment, we assume the expected channel gain as an increasing function of the number of independent multipaths K_{max}.

A. Asymptotical Performance With Varying K_{max}

Theorem 3 holds when K_{max} is sufficiently large. We first validate our theoretical analysis in Theorem 3 considering varying K_{max}. In the following, we assume W is so large that all K_{max} multipaths can be revealed. The y-axis is DR_j/W, where R_j is the expected achievable rate of the j^{th} receiver, D is the backoff factor and W is the system bandwidth. Since the channel gain is assumed to be an increasing function of K_{max}, the asymptotical performance would increase with K_{max} as well. The case when D is not sufficiently large, e.g., $D = K_{max}$ is first investigated. The expected asymptotical performance of each receiver is shown in Fig. 4 with $p_u = 5$dB and different N. From Fig. 4, we can observe that the performance using ZF and MMSE waveforms converges to the same limit quickly as K_{max} becomes sufficiently large. Also, there is a gap between the asymptotic limit of ZF/MMSE waveform and the lower bound of the basic TR waveform. This is mainly because when the basic TR waveform is used and the D is not large enough, there exists residual ISI and IUI and $\frac{\alpha\left(\sum_{k=1}^{K_{max}}\sigma_k^2\right)^2}{\|\mathbf{h}_j\|^2}$ cannot be negligible. By comparing the results with $N = 6$ and $N = 20$, we notice that the gap becomes even larger when N increases, which is due to the increase of $\alpha = 2N/D$.

We also compare the asymptotical performance of basic TR, ZF and MMSE waveforms with a larger D. It can be seen in Fig. 8 that the gap between the asymptotic performance of ZF/MMSE waveform and that of the basic TR waveform becomes much smaller when D and K_{max} are both sufficiently

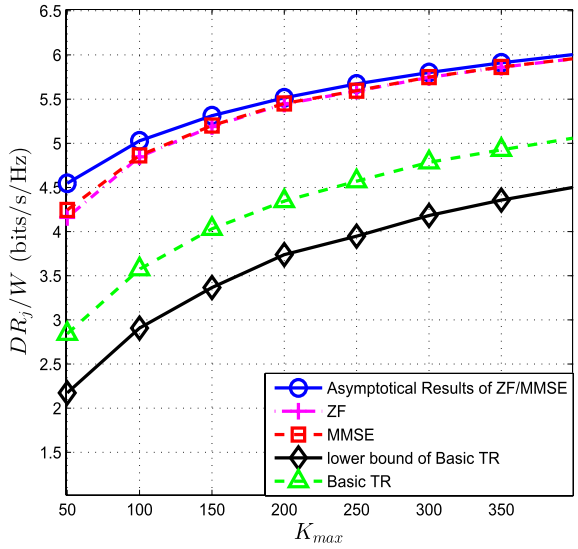

(a)

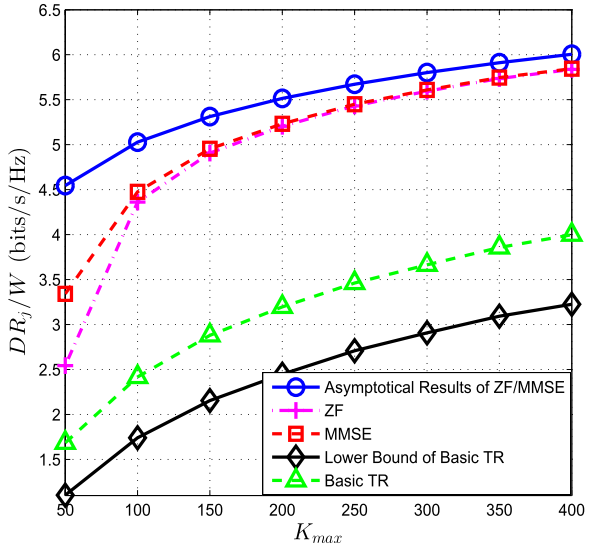

(b)

Fig. 4. The asymptotic performance with varying K_{max}, $D = K_{max}$ and $p_u = 5$dB. (a) $N = 6$. (b) $N = 20$.

larger. Such a phenomenon is mainly due to less severe ISI and IUI and a much smaller $\frac{\alpha\left(\sum_{k=1}^{K_{max}} \sigma_k^2\right)^2}{\|\mathbf{h}_j\|^2}$. Therefore, the basic TR waveform can achieve the same optimal asymptotic expected achievable rate with ZF and MMSE waveforms with sufficiently large D.

Note that p_u is fixed as 5dB in the simulations, which implies that the trend in Fig. 4 and Fig. 8 also applies to the energy efficiency. In other words, the energy efficiency of the TR system increases with K_{max}.

B. The Number of Observable Independent Multipaths K in a Typical Indoor Environment

To achieve the asymptotic performance in Theorem 3 requires the TR system to resolve a sufficiently large amount of multipaths in the environment. In this subsection,

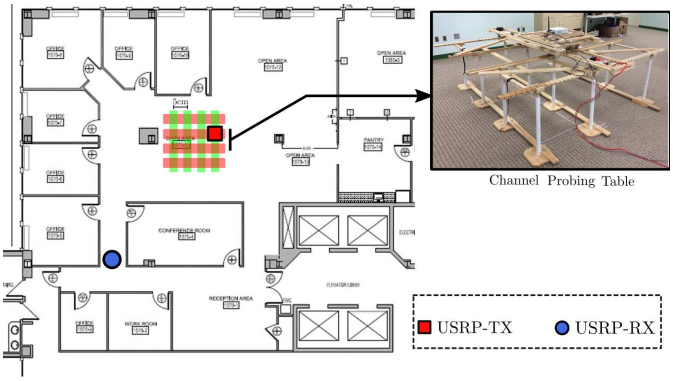

Fig. 5. The Floor Plan and Experiment Setting.

we investigate the property of K in a typical indoor environment using real-world measurements. First, we demonstrate that, in a typical office, the number of resolvable multipaths is large with a sufficiently large bandwidth. Then, the approach to increase K_{max} is further discussed and validated through real measurements.

We use two Universal Software Radio Peripherals (USRPs) as channel sounders to probe the channel in a typical office room, whose floor plan is shown in Fig. 5. As shown in the figure, TX is placed on a grid structure with 5cm resolution and RX is placed at the corner. With two USRPs, we scan the spectrum, e.g., from 4.9GHz to 5.9GHz, to acquire the channel impulse response with a bandwidth of 10MHz-1GHz.

We employ eigenvalue analysis to determine the value of K for any given bandwidth W. First, we estimate the covariance matrix of the measured channels $\mathbf{K}_{h,W}$ using statistical averaging

$$\mathbf{K}_{h,W} = \frac{1}{N}\sum_{i=1}^{N} \mathbf{h}_{i,W}\mathbf{h}_{i,W}^{\dagger}, \tag{19}$$

where $\mathbf{h}_{i,W}$ is the channel information obtained at location i with bandwidth W and $N = 100$. Since $\mathbf{K}_{h,W}$ is Hermitian and positive definite, there exists a unitary matrix U such that

$$\mathbf{K}_{h,W} = U\Lambda U^{\dagger} = \sum_{i=1}^{L} \lambda_{i,W}\psi_i\psi_i^{\dagger}, \tag{20}$$

where $\lambda_{1,W} \geq \lambda_{2,W} \geq \cdots \geq \lambda_{L,W}$ and $L = \tau_C W$.

In Fig. 6, we show the percentage of the captured energy E_l versus the number of significant eigenvalues l, with E_l defined as $E_l = \frac{\sum_{i=1}^{l}\lambda_i}{\sum_{i=1}^{L}\lambda_i}$. From Fig. 6, we can see that the channel energy is concentrated in a small number of eigenvalues when the bandwidth is small, while spread over a large number of eigenvalues as the bandwidth increases. In other words, the degree of freedom K increases as the bandwidth W increases. This is further confirmed in Fig. 7, where we show the number of significant eigenvalues versus the channel bandwidth by fixing the captured energy at 98%.

From previous measurements, K_{max} is a large value in a typical indoor environment. Now we discuss an approach to further increase K_{max} in practical environment. Since the TR and MIMO technology are not mutually exclusive, the

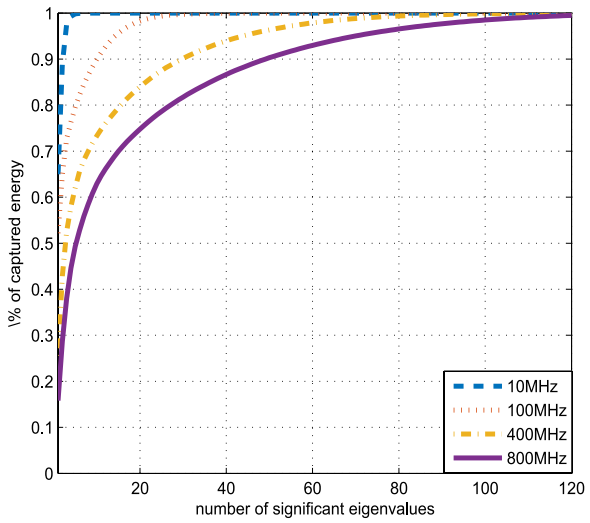

Fig. 6. Percentage of captured energy versus the number of significant eigenvalues.

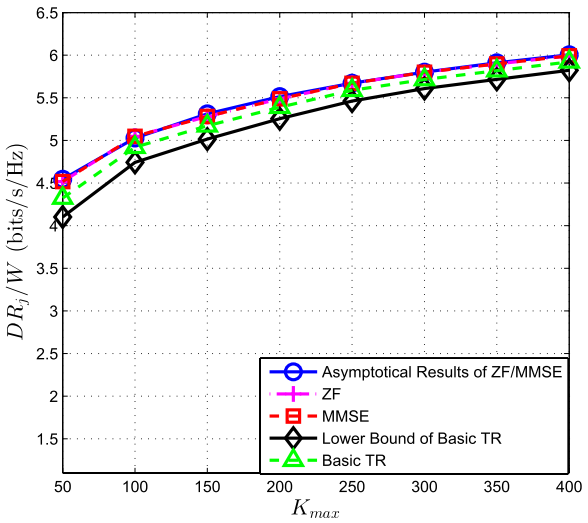

Fig. 8. The asymptotic performance with varying K_{max}, $D = K_{max}^{1.5}$, $N = 6$ and $p_u = 5$dB.

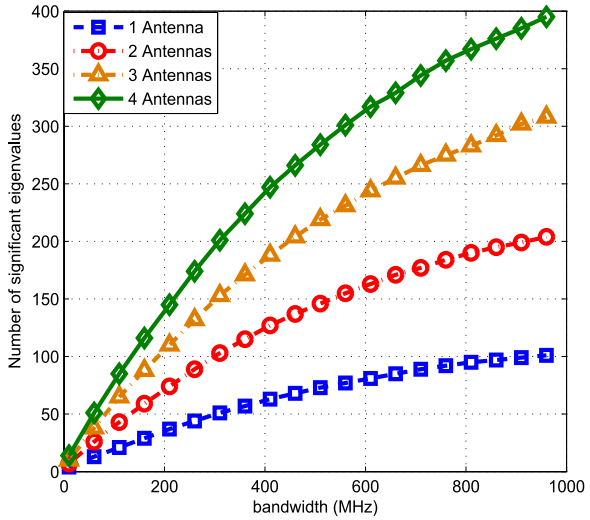

Fig. 7. Number of significant eigenvalues K at different bandwidth W.

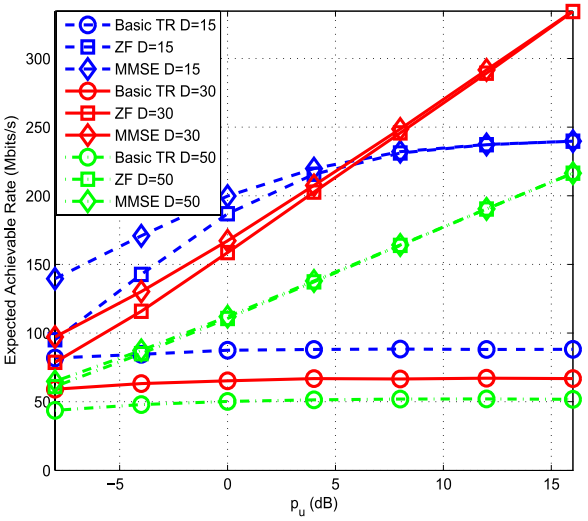

Fig. 9. Expected achievable rate with $N = 10$ and $W = 1$GHz.

degree of freedom can be further scaled up by deploying a couple antennas to harvest hundreds of virtual antennas as shown in Fig. 7. As indicated in the figure, it would be easy to realize massive virtual antennas with a few antennas in the TR system instead of installing hundreds of physical antennas.

C. Achievable Rate Evaluation

In the following, we will demonstrate that even with a single antenna, TR wideband system is still capable to reach a promising achievable rate based on our indoor experiment. Our experiment is conducted with the real indoor channel measurement and the achievable rate in TR system is calculated based on Theorem 2.

We first evaluate the expected achievable rate of the TR system in a typical indoor environment using the channel measurements in the previous subsection, with $W = 1$GHz. Then we compare the performance of the TR system with that of a massive MIMO system. Clearly, there is a tradeoff in selecting a proper D: W/D in Theorem 2 will decrease as D increases, while both the ISI and IUI get reduced as D increases. In Fig. 9 we show the the expected achievable rate of different waveforms with different D.

We can see that the expected achievable rate of the basic TR waveform saturates quickly as p_u increases because it is interference-limited with $N = 10$ receivers. Increasing D may decrease the expected achievable rate for the basic TR waveform if the decrease in W/D dominates the increase in SINR for a relatively large D as shown in Fig. 9. The expected achievable rates of ZF and MMSE waveforms also saturate at high p_u with $D = 15$, but can be improved by increasing D, e.g. $D = 30$, to reduce the interference. However, it may hurt the rate performance if we increase D too much, e.g., $D = 50$.

We choose $D = 30$ as the backoff factor used in the TR system to evaluate the achievable rate in a practical indoor environment, as shown in Fig. 10, which is comparable to a 20MHz massive MIMO system with around 500 transmit antennas.

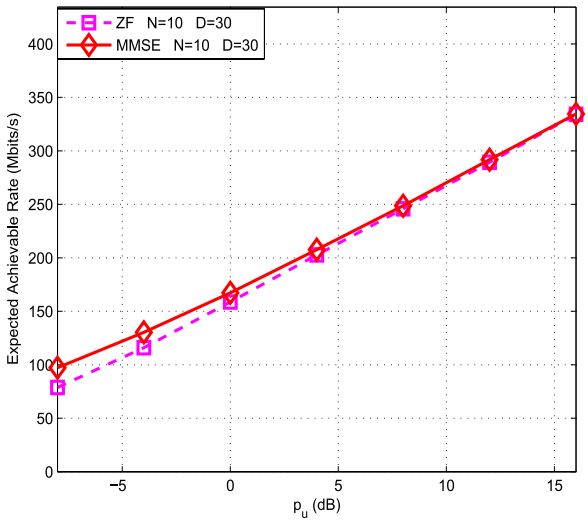

Fig. 10. Expected achievable rate with $W = 1$GHz, $N = 10$ and $D = 30$.

Fig. 11. A Time-reversal prototype.

Note that TR technology pays the price of spectral efficiency loss for the low cost and complexity implementation for indoor communications. For example, as shown in Fig. 11 [33], the TR prototype is a customized software defined radio (SDR) platform for designing and deploying TR-based communication systems. The size of the radio is 5cm by 17cm by 23cm, the weight is about 400g, and the power consumption is 25W. Compared with the massive MIMO prototype built in [9], the complexity and operation power consumption are obviously much lower. Considering the potential wide bandwidth available in future (e.g., UWB and mmWave band), the complexity, energy consumption and other metrics become more and more important compared with the spectral efficiency in indoor scenarios, which makes the TR technology a promising candidate for indoor communication.

VII. Conclusion

In this paper, we demonstrate that the TR technology, through harvesting the naturally existing virtual antennas, can offer a cost effective solution to realize the massive multipath effect, which is a counterpart of massive MIMO effect in indoor scenarios. With the derived massive multipath effect, we further derive the asymptotic rates of TR technology in a rich-scattering environment. We validate with simulations that the TR system with typical waveforms can achieve the limiting achievable rate with a sufficiently large amount of multipaths revealed. Finally, based on the real channel measurements, it is shown that the single-antenna TR wideband system can achieve promising rates in a practical indoor environment. By utilizing the environment as virtual antenna array and computing resource, the low complexity of TR technology is ideal for indoor communications. What a TR system needs is a large enough bandwidth to harvest the multipaths in the environment, which can be made possible with more affordable high-speed ADC and wide spectrum in mmWave band.

Appendix

A. Proof for Theorem 1

Proof: In a massive multipath environment, K_{max} is sufficiently large but finite. To reveal all the multipaths, we consider the asymptotic setting that $W \to \infty$. Notice that every element in $\mathbf{QQ}^\dagger$ is the sum of multiple independent variables, which converges to a Gaussian random variable in distribution when K_{max} is sufficiently large based on the central limit theorem. Since Gaussian random variable is only determined by the first and second moment and obviously each element in $\mathbf{QQ}^\dagger$ has zero mean, we only need to prove the largest variance of off-diagonal element will converge to zero.

Based on the definition of $\mathbf{Q}$, we have

$$\mathbf{QQ}^\dagger = \begin{bmatrix} \mathbf{H}_1\mathbf{H}_1^\dagger & \mathbf{H}_1\mathbf{H}_2^\dagger & \cdots & \mathbf{H}_1\mathbf{H}_N^\dagger \\ \mathbf{H}_2\mathbf{H}_1^\dagger & \mathbf{H}_2\mathbf{H}_2^\dagger & \cdots & \mathbf{H}_2\mathbf{H}_N^\dagger \\ \vdots & \vdots & \ddots & \cdots \\ \mathbf{H}_N\mathbf{H}_1^\dagger & \mathbf{H}_N\mathbf{H}_2^\dagger & \cdots & \mathbf{H}_N\mathbf{H}_N^\dagger \end{bmatrix}. \tag{21}$$

With (21), we can directly obtain

$$\left[\mathbf{QQ}^\dagger\right]_{l_j,l_j} = \mathbf{H}_j^{(\frac{L}{D})}\mathbf{H}_j^{(\frac{L}{D})\dagger} = \|\mathbf{h}_j\|^2, \tag{22}$$

where $[\cdot]_{m,n}$ represents the element in the m^{th} row and the n^{th} column of the matrix.

Then, we prove that $\mathbf{QQ}^\dagger$ is diagonal by examining the off-diagonal elements. Note that each off-diagonal matrix ($\forall i \neq j$) in (21), $\mathbf{H}_i\mathbf{H}_j^\dagger$, can be expanded as

$$\mathbf{H}_i\mathbf{H}_j^\dagger = \begin{bmatrix} \mathbf{H}_i^{(1)}\mathbf{H}_j^{(1)\dagger} & \mathbf{H}_i^{(1)}\mathbf{H}_j^{(2)\dagger} & \cdots & \mathbf{H}_i^{(1)}\mathbf{H}_j^{(\frac{2L-1}{D})\dagger} \\ \mathbf{H}_i^{(2)}\mathbf{H}_j^{(1)\dagger} & \mathbf{H}_i^{(2)}\mathbf{H}_j^{(2)\dagger} & \cdots & \mathbf{H}_i^{(2)}\mathbf{H}_j^{(\frac{2L-1}{D})\dagger} \\ \vdots & \vdots & \ddots & \cdots \\ \mathbf{H}_i^{(\frac{2L-1}{D})}\mathbf{H}_j^{(1)\dagger} & \mathbf{H}_i^{(\frac{2L-1}{D})}\mathbf{H}_j^{(2)\dagger} & \cdots & \mathbf{H}_i^{(\frac{2L-1}{D})}\mathbf{H}_j^{(\frac{2L-1}{D})\dagger} \end{bmatrix}. \tag{23}$$

From (23), we can see that each element of $\mathbf{H}_i\mathbf{H}_j^\dagger$, $\left[\mathbf{H}_i\mathbf{H}_j^\dagger\right]_{m,n} = \mathbf{H}_i^{(m)}\mathbf{H}_j^{(n)\dagger}$, is the sum of multiple independent random variables. Therefore, when K_{max} is sufficiently large, $\left[\mathbf{H}_i\mathbf{H}_j^\dagger\right]_{m,n}$ can be regarded as a Gaussian random variable, whose distribution is completely determined by the first and the second moments.

Based on the independence between the channel taps and distinct receivers, it is obvious that

$$\mathbb{E}\left[\mathbf{H}_i^{(m)}\mathbf{H}_j^{(n)\dagger}\right] = 0, \tag{24}$$

while the second moment can be upper bounded as follows

$$\begin{aligned}\mathbb{E}\left[|\mathbf{H}_i^{(m)}\mathbf{H}_j^{(n)\dagger}|^2\right] &\overset{(a)}{=} \sum_{l=1}^{L}\mathbb{E}\left[|\mathbf{H}_i^{(m)}(l)|^2|\mathbf{H}_j^{(n)}(l)|^2\right]\\ &\overset{(b)}{\leq} \sum_{l=1}^{L}\mathbb{E}\left[|\mathbf{H}_i^{(\frac{L}{D})}(l)|^2\right]\mathbb{E}\left[|\mathbf{H}_j^{(\frac{L}{D})}(l)|^2\right]\\ &\overset{(c)}{=} \frac{\left(\sum_{k=1}^{K_{max}}\sigma_k^2\right)^2}{L},\end{aligned} \tag{25}$$

where (a) is obtained directly from the independence, (b) is based on the matrix structure in (8) and (c) comes from the fact that the K_{max} multipaths are randomly distributed among the L-tap channel and thus

$$\mathbb{E}\left[|h_j(m)|^2\right] = \mathbb{E}\left[|h_j(n)|^2\right] = \frac{\sum_{k=1}^{K_{max}}\sigma_k^2}{L}, \quad \forall m,n. \tag{26}$$

Due to the path loss attenuation, $\sigma_k^2 \leq 1$, which means that $\sum_{k=1}^{K_{max}}\sigma_k^2 \leq K_{max}$. Under the asymptotic setting that $W \to \infty$, $L \to \infty$ according to the definition that $L = round(\tau_C W)$. Since K_{max} is finite, $K_{max}^2/L \to 0$ as $W \to \infty$, i.e., (c) goes to 0. From (24) and (25), we can conclude that

$$\left[\mathbf{H}_i\mathbf{H}_j^\dagger\right]_{m,n} \xrightarrow{d} 0, \quad \forall m,n, and\ i \neq j. \tag{27}$$

Next, let us examine the diagonal submatrix of $\mathbf{QQ}^\dagger$, which can be expanded as

$$\mathbf{H}_j\mathbf{H}_j^\dagger = \begin{bmatrix} \mathbf{H}_j^{(1)}\mathbf{H}_j^{(1)\dagger} & \mathbf{H}_j^{(1)}\mathbf{H}_j^{(2)\dagger} & \cdots & \mathbf{H}_j^{(1)}\mathbf{H}_j^{(\frac{2L-1}{D})\dagger} \\ \mathbf{H}_j^{(2)}\mathbf{H}_j^{(1)\dagger} & \mathbf{H}_j^{(2)}\mathbf{H}_j^{(2)\dagger} & \cdots & \mathbf{H}_j^{(2)}\mathbf{H}_j^{(\frac{2L-1}{D})\dagger} \\ \vdots & \vdots & \ddots & \cdots \\ \mathbf{H}_j^{(\frac{2L-1}{D})}\mathbf{H}_j^{(1)\dagger} & \mathbf{H}_j^{(\frac{2L-1}{D})}\mathbf{H}_j^{(2)\dagger} & \cdots & \mathbf{H}_j^{(\frac{2L-1}{D})}\mathbf{H}_j^{(\frac{2L-1}{D})\dagger} \end{bmatrix}. \tag{28}$$

Similarly, each element $\left[\mathbf{H}_j\mathbf{H}_j^\dagger\right]_{m,n} = \mathbf{H}_j^{(m)}\mathbf{H}_j^{(n)\dagger}$ can be regarded as Gaussian variable when K_{max} is sufficiently large. Since $\mathbf{H}_j^{(m)}$ and $\mathbf{H}_j^{(n)}$ are independent when $m \neq n$, similar to (24) and (25), we can derive

$$\begin{cases}\mathbb{E}\left[\mathbf{H}_j^{(m)}\mathbf{H}_j^{(n)\dagger}\right] = 0, & m \neq n,\\ \mathbb{E}\left[|\mathbf{H}_j^{(m)}\mathbf{H}_j^{(n)\dagger}|^2\right] \leq \frac{\left(\sum_{k=1}^{K_{max}}\sigma_k^2\right)^2}{L}, & m \neq n,\end{cases} \tag{29}$$

and given $K_{max}^2/L \to 0$ as $W \to \infty$, we have derived that

$$\left[\mathbf{H}_j\mathbf{H}_j^\dagger\right]_{m,n} \xrightarrow{d} 0, \quad \forall j, and\ m \neq n. \tag{30}$$

Therefore, we can conclude that $\mathbf{QQ}^\dagger$ is diagonal. This completes the proof. ■

B. Proof of Theorem 2

1) Expected Achievable Rate Under Basic TR Waveform: From (12), the basic TR waveform is $\mathbf{g}_j = \mathbf{H}_j^{(L/D)\dagger}/\|\mathbf{H}_j^{(L/D)}\|$. Therefore, we have

$$\mathbf{g}_j^\dagger\mathbf{H}_j^{(\frac{L}{D})\dagger}\mathbf{H}_j^{(\frac{L}{D})}\mathbf{g}_j = \|\mathbf{H}_j^{(\frac{L}{D})}\|^2, \tag{31}$$

and

$$\mathbf{g}_j^\dagger\left(\sum_{i=1}^{N}\mathbf{H}_i^\dagger\mathbf{H}_i\right)\mathbf{g}_j = \frac{\mathbf{H}_j^{(\frac{L}{D})}\mathbf{Q}^\dagger\mathbf{Q}\mathbf{H}_j^{(\frac{L}{D})\dagger}}{\|\mathbf{H}_j^{(\frac{L}{D})}\|^2}. \tag{32}$$

According to the definition of $\mathbf{H}_j^{(L/D)}$, we have $\|\mathbf{H}_j^{(\frac{L}{D})}\|^2 = \|\mathbf{h}_j\|^2$, and $\mathbf{H}_j^{(L/D)}$ is the $(L/D)^{th}$ row of $\mathbf{H}_j$ and thus l_j^{th} row of $\mathbf{Q}$. Therefore, (31) and (32) can be re-written as

$$\mathbf{g}_j^\dagger\mathbf{H}_j^{(\frac{L}{D})\dagger}\mathbf{H}_j^{(\frac{L}{D})}\mathbf{g}_j = \|\mathbf{h}_j\|^2, \tag{33}$$

and

$$\mathbf{g}_j^\dagger\left(\sum_{i=1}^{N}\mathbf{H}_i^\dagger\mathbf{H}_i\right)\mathbf{g}_j = \frac{\left[\mathbf{QQ}^\dagger\mathbf{QQ}^\dagger\right]_{l_j,l_j}}{\|\mathbf{h}_j\|^2}, \tag{34}$$

where $[\,\cdot\,]_{l_j,l_j}$ is the (l_j,l_j) element of the matrix.

Substituting (33) and (34) into (10), the expected achievable rate of j^{th} receiver with the basic TR waveform can be written as

$$R_j^{Basic} = \frac{W}{D}\mathbb{E}\left[\log_2\left(1 + \frac{p_u\|\mathbf{h}_j\|^4}{p_u([\mathbf{QQ}^\dagger\mathbf{QQ}^\dagger]_{l_j,l_j} - \|\mathbf{h}_j\|^4) + \|\mathbf{h}_j\|^2}\right)\right]. \tag{35}$$

2) Expected Achievable Rate Under ZF Waveform: With the ZF waveform $\mathbf{g}_j = c_{ZF}\mathbf{Q}^\dagger(\mathbf{QQ}^\dagger)^{-1}\mathbf{e}_{l_j}$, we have

$$\begin{bmatrix}\mathbf{H}_1\mathbf{g}_j\\ \vdots\\ \mathbf{H}_N\mathbf{g}_j\end{bmatrix} = \mathbf{Q}\mathbf{g}_j = c_{ZF}\mathbf{QQ}^\dagger(\mathbf{QQ}^\dagger)^{-1}\mathbf{e}_{l_j} = c_{ZF}\mathbf{e}_{l_j}. \tag{36}$$

According to (36), we can derive the following

$$\mathbf{g}_j^\dagger\mathbf{H}_i^\dagger\mathbf{H}_i\mathbf{g}_j = \begin{cases}0, & \forall i \neq j,\\ \mathbf{g}_j^\dagger\mathbf{H}_j^{(\frac{L}{D})\dagger}\mathbf{H}_j^{(\frac{L}{D})}\mathbf{g}_j = c_{ZF}^2, & i = j.\end{cases} \tag{37}$$

Substituting (37) into (10), we can see that both the ISI and IUI are eliminated, and thus the expected achievable rate with ZF waveform can be written as

$$R_j^{ZF} = \frac{W}{D}\mathbb{E}\left[\log_2\left(1 + p_u c_{ZF}^2\right)\right]. \tag{38}$$

$$R_j^{MMSE} \overset{(a)}{=} \frac{W}{D}\mathbb{E}\left[\log_2\left(1+\frac{\mathbf{g}_j^\dagger \mathbf{H}_j^{(\frac{L}{D})\dagger}\mathbf{H}_j^{(\frac{L}{D})}\mathbf{g}_j}{\mathbf{g}_j^\dagger\left(\mathbf{H}_j^\dagger\mathbf{H}_j-\mathbf{H}_j^{(\frac{L}{D})\dagger}\mathbf{H}_j^{(\frac{L}{D})}+\sum_{i\neq j}\mathbf{H}_i^\dagger\mathbf{H}_i+\frac{1}{p_u}\mathbf{I}\right)\mathbf{g}_j}\right)\right]$$
$$\overset{(b)}{=} \frac{W}{D}\mathbb{E}\left[\log_2\left(1+\frac{\mathbf{g}_j^\dagger \mathbf{H}_j^{(\frac{L}{D})\dagger}\mathbf{H}_j^{(\frac{L}{D})}\mathbf{g}_j}{\mathbf{g}_j^\dagger\Lambda_j\mathbf{g}_j}\right)\right]$$
$$\overset{(c)}{=} \frac{W}{D}\mathbb{E}\left[\log_2\left(1+\mathbf{H}_j^{(\frac{L}{D})}\Lambda_j^{-1}\mathbf{H}_j^{(\frac{L}{D})\dagger}\right)\right] \tag{40}$$

Since $\mathbf{g}_j^\dagger\mathbf{g}_j = c_{ZF}^2[(\mathbf{Q}\mathbf{Q}^\dagger)^{-1}]_{l_j,l_j} = 1$, the expected achievable rate with ZF waveform in (38) can be re-written as

$$R_j^{ZF} = \frac{W}{D}\mathbb{E}\left[\log_2\left(1+\frac{p_u}{[(\mathbf{Q}\mathbf{Q}^\dagger)^{-1}]_{l_j,l_j}}\right)\right]. \tag{39}$$

3) Expected Achievable Rate Under MMSE Waveform: According to (12) and the Woodbury matrix identity [39], the MMSE waveform can be written as

$$\mathbf{g}_j = c_{MMSE}\left(\mathbf{Q}^\dagger\mathbf{Q}+\frac{1}{p_u}\mathbf{I}\right)^{-1}\mathbf{H}_j^{(\frac{L}{D})\dagger} = \frac{c_{MMSE}\Lambda_j^{-1}\mathbf{H}_j^{(\frac{L}{D})\dagger}}{\mathbf{H}_j^{(\frac{L}{D})}\Lambda_j^{-1}\mathbf{H}_j^{(\frac{L}{D})\dagger}+1}, \tag{41}$$

where $\Lambda_j \triangleq \mathbf{Q}^\dagger\mathbf{Q} - \mathbf{H}_j^{(\frac{L}{D})\dagger}\mathbf{H}_j^{(\frac{L}{D})} + (1/p_u)\mathbf{I}$.

By multiplying both sides in (41) with $\mathbf{H}_j^{(\frac{L}{D})}$, we can derive the following

$$\mathbf{H}_j^{(\frac{L}{D})}\Lambda_j^{-1}\mathbf{H}_j^{(\frac{L}{D})\dagger} = \frac{1}{1-\mathbf{H}_j^{(\frac{L}{D})}\left(\mathbf{Q}^\dagger\mathbf{Q}+\frac{1}{p_u}\mathbf{I}\right)^{-1}\mathbf{H}_j^{(\frac{L}{D})\dagger}} - 1. \tag{42}$$

Moreover, according to (41), we have

$$\mathbf{g}_j^\dagger\mathbf{H}_j^{(\frac{L}{D})\dagger}\mathbf{H}_j^{(\frac{L}{D})}\mathbf{g}_j = \frac{c_{MMSE}^2\left(\mathbf{H}_j^{(\frac{L}{D})}\Lambda_j^{-1}\mathbf{H}_j^{(\frac{L}{D})\dagger}\right)^2}{\left(\mathbf{H}_j^{(\frac{L}{D})}\Lambda_j^{-1}\mathbf{H}_j^{(\frac{L}{D})\dagger}+1\right)^2}, \tag{43}$$

and

$$\mathbf{g}_j^\dagger\Lambda_j\mathbf{g}_j = \frac{c_{MMSE}^2\mathbf{H}_j^{(\frac{L}{D})}\Lambda_j^{-1}\mathbf{H}_j^{(\frac{L}{D})\dagger}}{\left(\mathbf{H}_j^{(\frac{L}{D})}\Lambda_j^{-1}\mathbf{H}_j^{(\frac{L}{D})\dagger}+1\right)^2}. \tag{44}$$

Then, the expected achievable rate in (10) can be re-rewritten in (40), as shown at the top of this page, where (a) is the direct result from $\mathbf{g}_j^\dagger\mathbf{g}_j = 1$, (b) comes from the definition of Λ_j, and (c) are based on (43) and (44).

By substituting (42) into (40), the expected achievable rate with MMSE waveform can be further simplified as

$$R_j^{MMSE} = \frac{W}{D}\mathbb{E}\left[\log_2\left(\frac{1}{1-\mathbf{H}_j^{(\frac{L}{D})}\left(\mathbf{Q}^\dagger\mathbf{Q}+\frac{1}{p_u}\mathbf{I}\right)^{-1}\mathbf{H}_j^{(\frac{L}{D})\dagger}}\right)\right]$$
$$= \frac{W}{D}\mathbb{E}\left[\log_2\left(\frac{1}{1-\left[\mathbf{Q}\left(\mathbf{Q}^\dagger\mathbf{Q}+\frac{1}{p_u}\mathbf{I}\right)^{-1}\mathbf{Q}^\dagger\right]_{l_j,l_j}}\right)\right]$$
$$= \frac{W}{D}\mathbb{E}\left[\log_2\left(\frac{1}{\left[\left(\mathbf{I}+p_u\mathbf{Q}\mathbf{Q}^\dagger\right)^{-1}\right]_{l_j,l_j}}\right)\right], \tag{45}$$

where the second equality comes from the definition of $\mathbf{H}_j^{(\frac{L}{D})}$ and the last equality comes from the following derivation by utilizing the Woodbury matrix identity [39],

$$\left(\mathbf{I}+p_u\mathbf{Q}\mathbf{Q}^\dagger\right)^{-1} = \mathbf{I}-\mathbf{Q}\left(\frac{1}{p_u}\mathbf{I}+\mathbf{Q}^\dagger\mathbf{Q}\right)^{-1}\mathbf{Q}^\dagger. \tag{46}$$

Up to now, we have derived the expected achievable rate under different designs of waveform, and the results are summarized in Theorem 2.

C. Proof of Lemma 1

Proof: With the definition of $\mathbf{Q}$ and (9), we have

$$\left[\mathbf{Q}\mathbf{Q}^\dagger\mathbf{Q}\mathbf{Q}^\dagger\right]_{l_j,l_j} - \|\mathbf{h}_j\|^4 = \sum_{i=1,i\neq j}^{N}\sum_{l=1}^{(2L-1)/D}|\mathbf{H}_i^{(l)}\mathbf{H}_j^{(\frac{L}{D})\dagger}|^2 + \sum_{l=1,l\neq(L/D)}^{(2L-1)/D}|\mathbf{H}_j^{(l)}\mathbf{H}_j^{(\frac{L}{D})\dagger}|^2, \tag{47}$$

which is the sum of multiple independent random variables. Therefore, $\left[\mathbf{Q}\mathbf{Q}^\dagger\mathbf{Q}\mathbf{Q}^\dagger\right]_{l_j,l_j} - \|\mathbf{h}_j\|^4$ can be regarded as a Guassian random variable when K_{max} is sufficiently large.

Similar to (25), we have the following

$$\begin{cases}\mathbb{E}\left[|\mathbf{H}_i^{(l)}\mathbf{H}_j^{(\frac{L}{D})\dagger}|^2\right] \leq \frac{\left(\sum_{k=1}^{K_{max}}\sigma_k^2\right)^2}{L}, & i\neq j,\\ \mathbb{E}\left[|\mathbf{H}_j^{(l)}\mathbf{H}_j^{(\frac{L}{D})\dagger}|^2\right] \leq \frac{\left(\sum_{k=1}^{K_{max}}\sigma_k^2\right)^2}{L}, & l\neq(L/D).\end{cases} \tag{48}$$

Therefore, the expectation of $\left[\mathbf{Q}\mathbf{Q}^{\dagger}\mathbf{Q}\mathbf{Q}^{\dagger}\right]_{l_j,l_j} - \|\mathbf{h}_j\|^4$ can be bounded by

$$\mathbb{E}\left[\left[\mathbf{Q}\mathbf{Q}^{\dagger}\mathbf{Q}\mathbf{Q}^{\dagger}\right]_{l_j,l_j} - \|\mathbf{h}_j\|^4\right] \le \frac{N(2L-1)}{D}\frac{\left(\sum_{k=1}^{K_{max}}\sigma_k^2\right)^2}{L} \le \alpha\left(\sum_{k=1}^{K_{max}}\sigma_k^2\right)^2, \quad (49)$$

with $\alpha = 2N/D$.

Similar to the argument in the derivation of (26), the fourth moment of $h_j(m)$ can be given as

$$\mathbb{E}\left[|h_j(m)|^4\right] = \mathbb{E}\left[|h_j(n)|^4\right] = 2\left(\frac{\sum_{k=1}^{K_{max}}\sigma_k^2}{L}\right)^2, \quad \forall m, n. \quad (50)$$

Then, we have,

$$\begin{cases} \mathbb{E}\left[|\mathbf{H}_i^{(l)}\mathbf{H}_j^{(\frac{L}{D})\dagger}|^4\right] \le \frac{4\left(\sum_{k=1}^{K_{max}}\sigma_k^2\right)^4}{L^3}, & i \ne j, \\ \mathbb{E}\left[|\mathbf{H}_j^{(l)}\mathbf{H}_j^{(\frac{L}{D})\dagger}|^4\right] \le \frac{4\left(\sum_{k=1}^{K_{max}}\sigma_k^2\right)^4}{L^3}, & l \ne (L/D). \end{cases} \quad (51)$$

Note $\sum_{k=1}^{K_{max}}\sigma_k^2 \le K_{max}$ holds due to path loss attenuation. Moreover, $K_{max}^2/L \to 0$ as $W \to \infty$. Therefore, the variance of $\left[\mathbf{Q}\mathbf{Q}^{\dagger}\mathbf{Q}\mathbf{Q}^{\dagger}\right]_{l_j,l_j} - \|\mathbf{h}_j\|^4$ goes to zero as $W \to \infty$ in the multipath-rich scenario. Combining the first moment in (49), we can derive the result in Lemma 1. This completes the proof. ∎

D. Proof of Theorem 3

Proof: According to the TRMME, we have

$$\frac{\left[\left(\mathbf{Q}\mathbf{Q}^{\dagger}\right)^{-1}\right]_{l_j,l_j}}{\|\mathbf{h}_j\|^2} \xrightarrow{d} 1, \quad (52)$$

since the inverse of a diagonal matrix should be diagonal.

Then, according to (39), the asymptotic expected achievable rate under ZF waveform is

$$\lim_{W\to\infty}\frac{R_j^{ZF}}{W/D} = \mathbb{E}\left[\log_2\left(1 + p_u\|\mathbf{h}_j\|^2\right)\right]. \quad (53)$$

Similarly, with the TRMME, we can also have

$$\left[\left(\mathbf{I} + p_u\mathbf{Q}\mathbf{Q}^{\dagger}\right)^{-1}\right]_{l_j,l_j} \xrightarrow{d} \left[(\mathbf{I} + p_u\lambda)^{-1}\right]_{l_j,l_j} = \frac{1}{1 + p_u\|\mathbf{h}_j\|^2}. \quad (54)$$

By substituting (54) into (45), the asymptotic expected achievable rate under MMSE waveform is

$$\lim_{W\to\infty}\frac{R_j^{MMSE}}{W/D} = \mathbb{E}\left[\log_2\left(1 + p_u\|\mathbf{h}_j\|^2\right)\right]. \quad (55)$$

Finally, by substituting (16) of Lemma 1 into (35), the asymptotic expected achievable rate under basic TR waveform can be lower bounded as

$$\lim_{W\to\infty}\inf\frac{R_j^{Basic}}{W/D} = \mathbb{E}\left[\log_2\left(1 + \frac{p_u\|\mathbf{h}_j\|^2}{\frac{p_u\alpha\left(\sum_{k=1}^{K_{max}}\sigma_k^2\right)^2}{\|\mathbf{h}_j\|^2} + 1}\right)\right]. \quad (56)$$

This completes the proof. ∎

REFERENCES

[1] "Visual networking index," Cisco, San Jose, CA, USA, Cisco White Paper 1454457600809267, 2016.

[2] J. G. Andrews *et al.*, "What will 5G be?" *IEEE J. Sel. Areas Commun.*, vol. 32, no. 6, pp. 1065–1082, Jun. 2014.

[3] H. Q. Ngo, E. G. Larsson, and T. L. Marzetta, "Energy and spectral efficiency of very large multiuser MIMO systems," *IEEE Trans. Commun.*, vol. 61, no. 4, pp. 1436–1449, Apr. 2013.

[4] T. L. Marzetta, "Noncooperative cellular wireless with unlimited numbers of base station antennas," *IEEE Trans. Wireless Commun.*, vol. 9, no. 11, pp. 3590–3600, Nov. 2010.

[5] F. Boccardi, R. W. Heath, A. Lozano, T. L. Marzetta, and P. Popovski, "Five disruptive technology directions for 5G," *IEEE Commun. Mag.*, vol. 52, no. 2, pp. 74–80, Feb. 2014.

[6] J. Liu, H. Minn, and A. Gatherer. (Jun. 2015). *Analog Front End Design Challenges for 5G Massive MIMO* [Online]. Available: http://www.comsoc.org/ctn/death-5g-part-2-will-analog-be-death-massive-mimo

[7] X. Artiga, B. Devillers, and J. Perruisseau-Carrier, "Mutual coupling effects in multi-user massive MIMO base stations," in *Proc. IEEE APSURSI*, Jul. 2012, pp. 1–2.

[8] C. Masouros, M. Sellathurai, and T. Ratnarajah, "Large-scale MIMO transmitters in fixed physical spaces: The effect of transmit correlation and mutual coupling," *IEEE Trans. Commun.*, vol. 61, no. 7, pp. 2794–2804, Jul. 2013.

[9] J. Vieira *et al.*, "A flexible 100-antenna testbed for massive MIMO," in *Proc. IEEE GC Wkshps*, Dec. 2014, pp. 287–293.

[10] M. Panolini. (Mar. 2011). *Beyond Data Caps: An Analysis of the Uneven Growth in Data Traffic*. [Online]. Available: http://www.senzafiliconsulting.com/

[11] R. Saadane, A. Menouni, R. Knopp, and D. Aboutajdine, "Empirical eigenanalysis of indoor UWB propagation channels," in *Proc. IEEE Global Telecommun. Conf. (GLOBECOM)*, vol. 5. Nov. 2004, pp. 3215–3219.

[12] A. M. Hayar, R. Knopp, and R. Saadane, "Subspace analysis of indoor UWB channels," *EURASIP J. Appl. Signal Process.*, vol. 2005, no. 3, pp. 287–295, Jan. 2005.

[13] A. Inamdar *et al.*, "Progress in design of improved high dynamic range analog-to-digital converters," *IEEE Trans. Appl. Supercond.*, vol. 19, no. 3, pp. 670–675, Jun. 2009.

[14] T. S. Rappaport *et al.*, "Millimeter wave mobile communications for 5G cellular: It will work!" *IEEE Access*, vol. 1, pp. 335–349, May 2013.

[15] P. F. M. Smulders and L. M. Correia, "Characterisation of propagation in 60 GHz radio channels," *Electron. Commun. Eng. J.*, vol. 9, no. 2, pp. 73–80, Apr. 1997.

[16] F. Han, Y.-H. Yang, B. Wang, Y. Wu, and K. J. R. Liu, "Time-reversal division multiple access over multi-path channels," *IEEE Trans. Commun.*, vol. 60, no. 7, pp. 1953–1965, Jul. 2012.

[17] B. Bogert, "Demonstration of delay distortion correction by time-reversal techniques," *IRE Trans. Commun. Syst.*, vol. 5, no. 3, pp. 2–7, Dec. 1957.

[18] A. Derode, P. Roux, and M. Fink, "Robust acoustic time reversal with high-order multiple scattering," *Phys. Rev. Lett.*, vol. 75, pp. 4206–4209, Dec. 1995.

[19] H. T. Nguyen, J. B. Andersen, and G. F. Pedersen, "The potential use of time reversal techniques in multiple element antenna systems," *IEEE Commun. Lett.*, vol. 9, no. 1, pp. 40–42, Jan. 2005.

[20] R. L. de L. Neto, A. M. Hayar, and M. Debbah, "Channel division multiple access based on high UWB channel temporal resolution," in *Proc. IEEE VTC*, Sep. 2006, pp. 1–5.

[21] B. Wang, Y. Wu, F. Han, Y.-H. Yang, and K. J. R. Liu, "Green wireless communications: A time-reversal paradigm," *IEEE J. Sel. Areas Commun.*, vol. 29, no. 8, pp. 1698–1710, Sep. 2011.

[22] M.-A. Bouzigues, I. Siaud, M. Helard, and A.-M. Ulmer-Moll, "Turn back the clock: Time reversal for green radio communications," *IEEE Veh. Technol. Mag.*, vol. 8, no. 1, pp. 49–56, Mar. 2013.

[23] Y. Jin, Y. Jiang, and J. M. F. Moura, "Multiple antenna time reversal transmission in ultra-wideband communications," in *Proc. IEEE GlOBECOM*, Nov. 2007, pp. 3029–3033.

[24] Y. H. Yang, B. Wang, W. S. Lin, and K. J. R. Liu, "Near-optimal waveform design for sum rate optimization in time-reversal multiuser downlink systems," *IEEE Trans. Wireless Commun.*, vol. 12, no. 1, pp. 346–357, Jan. 2013.

[25] E. Yoon, S. Y. Kim, and U. Yun, "A time-reversal-based transmission using predistortion for intersymbol interference alignment," *IEEE Trans. Commun.*, vol. 63, no. 2, pp. 455–465, Feb. 2015.

[26] Y. Chen *et al.*, "Time-reversal wireless paradigm for green Internet of Things: An overview," *IEEE Internet Things J.*, vol. 1, no. 1, pp. 81–98, Feb. 2014.
[27] I. H. Azzam and R. S. Adve, "Linear precoding for multiuser MIMO systems with multiple base stations," in *Proc. IEEE ICC*, Jun. 2009, pp. 1–6.
[28] L. Kewen, M. Zherui, and H. Ting, "A novel TR-STBC-OFDM scheme for mobile WiMAX system," in *Proc. IEEE 8th ISAPE*, Nov. 2008, pp. 1365–1368.
[29] M. Maaz, M. Helard, P. Mary, and M. Liu, "Performance analysis of time-reversal based precoding schemes in MISO-OFDM systems," in *Proc. IEEE 81st VTC*, May 2015, pp. 1–6.
[30] A. Pitarokoilis, S. K. Mohammed, and E. G. Larsson, "Uplink performance of time-reversal MRC in massive MIMO systems subject to phase noise," *IEEE Trans. Wireless Commun.*, vol. 14, no. 2, pp. 711–723, Feb. 2015.
[31] C. Zhou, N. Guo, B. M. Sadler, and R. C. Qiu, "Performance study on time reversed impulse MIMO for UWB communications based on measured spatial UWB channels," in *Proc. IEEE MILCOM*, Oct. 2007, pp. 1–6.
[32] B. M. Popovic, "Efficient Golay correlator," *Electron. Lett.*, vol. 35, no. 17, pp. 1427–1428, Aug. 1999.
[33] Z. H. Wu, Y. Han, Y. Chen, and K. J. R. Liu, "A time-reversal paradigm for indoor positioning system," *IEEE Trans. Veh. Technol.*, vol. 64, no. 4, pp. 1331–1339, Apr. 2015.
[34] R. C. Daniels and R. W. Heath, "Improving on time-reversal with MISO precoding," in *Proc. 8th Int. Symp. Wireless Pers. Commun. Conf.*, 2005, pp. 18–22.
[35] D. N. C. Tse and P. Viswanath, "Downlink-uplink duality and effective bandwidths," in *Proc. IEEE ISIT*, Jul. 2002, p. 52.
[36] M. Schubert and H. Boche, "Solution of the multiuser downlink beamforming problem with individual SINR constraints," *IEEE Trans. Veh. Technol.*, vol. 53, no. 1, pp. 18–28, Jan. 2004.
[37] R. Hunger and M. Joham, "A general rate duality of the MIMO multiple access channel and the MIMO broadcast channel," in *Proc. IEEE Global Telecommun. Conf.*, Nov./Dec. 2008, pp. 1–5.
[38] E. Telatar, "Capacity of multi-antenna Gaussian channels," *Eur. Trans. Telecommun.*, vol. 10, no. 6, pp. 585–595, 1999.
[39] G. H. Golub and C. F. Van Loan, *Matrix Computations*, vol. 3. Baltimore, MD, USA: The Johns Hopkins Univ. Press, 2012.

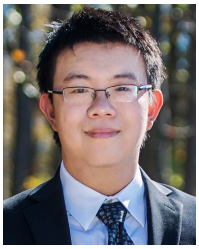

Yi Han received the B.S. degree in electrical engineering (highest honor) from Zhejiang University, Hangzhou, China, in 2011. He is currently pursuing the Ph.D. degree with the Department of Electrical and Computer Engineering, University of Maryland, College Park, MD, USA.

His research interests include wireless communication and signal processing. He was a recipient of Class A Scholarship from Chu Kochen Honors College, Zhejiang University, in 2008. He was also a recipient of the Best Student Paper Award at the IEEE ICASSP in 2016.

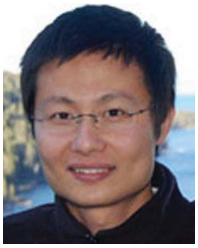

Yan Chen (SM'14) received the bachelor's degree from the University of Science and Technology of China in 2004, the M.Phil. degree from the Hong Kong University of Science and Technology in 2007, and the Ph.D. degree from the University of Maryland, College Park, MD, USA, in 2011. Being a Founding Member, he joined Origin Wireless Inc., as a Principal Technologist in 2013. He is currently a Professor with the University of Electronic Science and Technology of China. His research interests include multimedia, signal processing, game theory, and wireless communications.

He was the recipient of multiple honors and awards, including the Best Student Paper Award at the IEEE ICASSP in 2016, the best paper award at the IEEE GLOBECOM in 2013, the Future Faculty Fellowship and Distinguished Dissertation Fellowship Honorable Mention from the Department of Electrical and Computer Engineering in 2010 and 2011, the Finalist of the Dean's Doctoral Research Award from the A. James Clark School of Engineering, the University of Maryland in 2011, and the Chinese Government Award for outstanding students abroad in 2010.

Beibei Wang (SM'15) received the B.S. degree (highest honor) in electrical engineering from the University of Science and Technology of China, Hefei, in 2004, and the Ph.D. degree in electrical engineering from the University of Maryland, College Park, in 2009. She was with the University of Maryland as a Research Associate from 2009 to 2010, and with Qualcomm Research and Development from 2010 to 2014. Since 2015, she has been with Origin Wireless Inc. as a Principle Technologist. Her research interests include wireless communications and signal processing. She received the Graduate School Fellowship, the Future Faculty Fellowship, and the Dean's Doctoral Research Award from the University of Maryland, and the Overview Paper Award from IEEE Signal Processing Society in 2015. She is a co-author of *Cognitive Radio Networking and Security: A Game-Theoretic View* (Cambridge University Press, 2010).

K. J. Ray Liu (F'03) was named a Distinguished Scholar-Teacher with the University of Maryland, College Park, in 2007, where he is currently a Christine Kim Eminent Professor of Information Technology. He leads the Maryland Signals and Information Group conducting research encompassing broad areas of information and communications technology with recent focus on future wireless technologies, network science, and information forensics, and security.

Dr. Liu is a fellow of AAAS. He was a recipient of the 2016 IEEE Leon K. Kirchmayer Technical Field Award on graduate teaching and mentoring, the IEEE Signal Processing Society 2014 Society Award, and the IEEE Signal Processing Society 2009 Technical Achievement Award. He is recognized by Thomson Reuters as a Highly Cited Researcher.

Dr. Liu is a member of IEEE Board of Director. He was President of the IEEE Signal Processing Society, where he has served as Vice President - Publications and Board of Governor. He has also served as the Editor-in-Chief of *IEEE Signal Processing Magazine*.

He also received teaching and research recognitions from the University of Maryland, including the University-level Invention of the Year Award, and the college-level Poole and Kent Senior Faculty Teaching Award, the Outstanding Faculty Research Award, and the Outstanding Faculty Service Award from A. James Clark School of Engineering.